Phase separation in binary hard-core mixtures

Marjolein Dijkstra and Daan Frenkel
FOM Institute for Atomic and Molecular Physics, Kruislaan 407, 1098 SJ Amsterdam, The Netherlands

Jean-Pierre Hansen
Laboratoire de Physique, Unité de recherche 1325 Associée au CNRS, Ecole Normale Supérieure de Lyon, 46, Allée d'Italie, 69364 Lyon Cédex 07, France

(Received 14 March 1994; accepted 1 April 1994)

We report the observation of a purely entropic demixing transition in a three-dimensional binary hard-core mixture by computer simulations. This transition is observed in a lattice model of a binary hard-core mixture of parallel cubes provided that the size asymmetry of the large and small particles is sufficiently large ($\geqslant 3$, in the present case). In addition, we have performed simulations of a single athermal polymer in a hard-core solvent. As we increase the chemical potential of the solvent, we observe a purely entropy-driven collapse of the polymer: the scaling of the radius of gyration R_g of the polymer with the number of segments N changes from that of a polymer in a good solvent to that of a collapsed polymer. Both for the study of the hard-core demixing and of the polymer collapse, it was essential to use novel collective Monte Carlo moves to speed up equilibration. We show that in the limit $\sigma_1/\sigma_2 \rightarrow 0$, the pair distribution function for an off-lattice binary hard-core mixture of parallel cubes with side lengths σ_1 and σ_2 diverges at contact for the large particles. For the lattice system, we calculated the pair distribution functions $g(r)$ up to the fourth virial coefficient. The difference in $g(r)$ at contact for a binary system and a pure system at the same packing fraction gives a rough criterion, whether the mixture phase separates.

I. INTRODUCTION

One of the most striking phenomena in mixtures is phase separation. Until recently, it was generally believed that phase separation in simple mixtures is induced by energetic effects. An important question is therefore whether a phase separation can take place in an "athermal" mixture, i.e., a mixture for which the energy of mixing depends linearly on composition. The simplest model for an athermal mixture is a binary system containing large and small hard spheres. In 1964, Lebowitz and Rowlinson[3] showed that, within the Percus–Yevick closure of the Ornstein–Zernike equation, fluid hard sphere mixtures are stable with respect to phase separation. Thus far, computer simulations[4–8] found no evidence for fluid–fluid phase separation in additive hard sphere mixtures. In this context, additive means $\sigma_{AB}=(\sigma_{AA}+\sigma_{BB})/2$, where σ_{ij} denotes the distance of closest approach of particles of type i and j. In contrast, it is usually possible to have phase separation in a mixture with positive nonadditivity, i.e., $\sigma_{AB}>(\sigma_{AA}+\sigma_{BB})/2$,[9–11] because for such systems, the pure phases can fill space more effectively than the mixture. However, recently Biben and Hansen[12] showed that within the Rogers–Young closure of the Ornstein–Zernike equation, additive hard sphere mixtures will be unstable at high densities for diameter ratios larger than 5. For hard spheres, this thermodynamically self-consistent closure is known to be more accurate than the Percus–Yevick approximation. Similar predictions have subsequently been made using other approximations.[13] In principle, computer simulation is a suitable tool to investigate whether phase separation can take place in purely athermal mixtures. Unfortunately, direct simulation of phase separation in mixtures of very dissimilar spheres is difficult because of slow equilibration.[14] The numerical difficulties are less severe for lattice models of hard-core mixtures. We have therefore performed simulations of lattice models of additive hard-core particles.

The results of grand canonical Monte Carlo simulations of a mixture of large and small cubes with side ratios of 2 or 3 on a cubic lattice are reported in this paper. In Sec. II, the simulation method is discussed and the results are presented. The more technical aspects of the simulation method are explained in the Appendices. A question related to phase separation induced by purely entropic effects is whether an athermal polymer in a hard-core solvent undergoes a collapse transition. The results of a simulation of an athermal polymer in a hard-core solvent are reported in Sec. III. In Sec. IV, we show that in an off-lattice system of large and small parallel cubes, the pair distribution function of the large cubes diverges at contact in the limit $\sigma_1/\sigma_2 \rightarrow 0$, where σ_1 and σ_2 are the side lengths of the cubes. This tendency of the large cubes to stick together is strongly suggestive of phase separation. For the lattice system, we computed the pair distribution functions of the binary hard-cube mixture and compared them with the pair distribution functions for a pure system at the same packing fraction.

II. COMPUTER SIMULATIONS OF A BINARY MIXTURE OF HARD PARALLEL CUBES

A. Simulation method

The model that we consider is a mixture of large and small parallel hard cubes on a lattice. The diameter of each cube corresponds to an even number of lattice spacings. This model is clearly additive: at close packing we can fill space just as well in the mixed phase as in the pure phases. Hence there is no trivial volume-driven demixing. In our simulations, we considered mixtures of cubes with side ratios of 2

or 3 on a lattice with, respectively, 28×28×28 and 30×30×30 lattice points. In both cases, the side of the small cubes is equal to 2. We performed grand-canonical Monte Carlo (GCMC) simulations, where the independent variables are the fugacities of the large and the small cubes z_l and z_s. Three types of trial moves can be performed:

(i) random displacement of a particle in the box;

(ii) changing the identity of a particle (large to small or vice versa);

(iii) removal or insertion of a particle.

However, the acceptance ratio for a random displacement of a large particle is small in a dense system of small particles, as the displacement of a large particle is strongly hindered by the small particles. In order to speed up equilibration, we used collective particle moves that employed a generalization of the configurational-bias Monte Carlo scheme of Ref. 15. In this approach, the large particle was moved to a random trial position. Typically several small particles would occupy this region in space. These particles were then moved to the volume vacated by the large particle and inserted using Rosenbluth sampling.[14] The trial move was then accepted with a probability determined by the ratio of the Rosenbluth weights of the new and old configurations. Of course, a trial move would be rejected immediately if it resulted in overlap of two or more large particles. In order to investigate the influence of the surface-to-volume ratio on phase separation, we also performed simulations of a three-dimensional system of hard parallel platelets (size 6×6×2) and cubes (size 2×2×2) on a cubic lattice of 30×30×30. For the sake of comparison, we also simulated a two-dimensional mixture of hard squares (size 6×6 and 2×2) and a two-dimensional system of hard squares (size 2×2) and parallel hard rods (18×2).

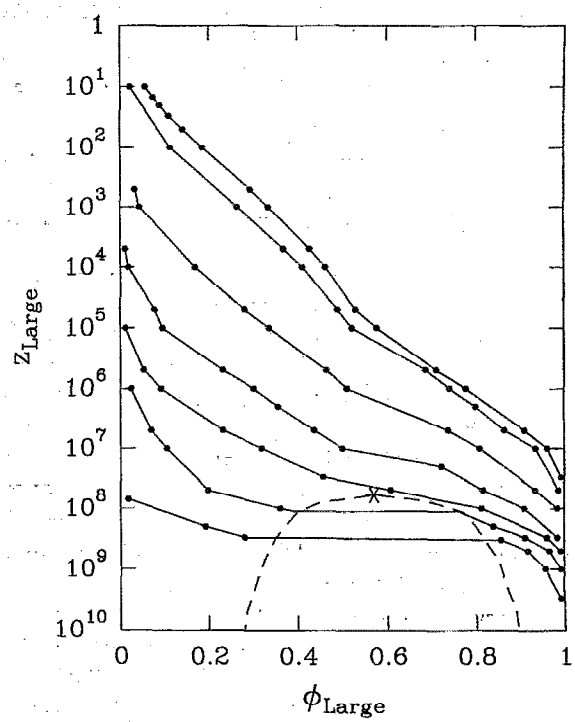

FIG. 1. The fugacity of the large cubes (size 6×6×6) vs the volume fraction of the large cubes at different fugacities (z_s=0, 100, 500, 1×10^3, 1.5×10^3, 2×10^3, and 5×10^3) of the small particles (size 2×2×2). The star denotes the critical point (z_l=6.02×10^7, z_s=1.63×10^3, and ϕ_{large}=0.57) and is derived by a global fit of all isofugacity curves. The rest of the binodal (dashed) curve could not be estimated as accurately as the critical point. This curve should therefore reconsidered as a guide to the eye.

B. Results

GCMC simulations were performed on a mixture of large and small cubes for a range of different values for the fugacities z_l and z_s. In each simulation, we computed the volume fractions of the large and small cubes. To allow faster equilibration, subsequent runs were started from previously equilibrated configurations at a higher or lower fugacity. Most runs consisted of 1×10^5–1×10^6 cycles per particle. In each cycle, we attempt a random displacement of a particle in the box, and we try to change the identity of a random particle. Once every ten cycles, a removal or insertion of a particle in the box is attempted. In Figs. 1 and 2, the fugacity of the large cubes is plotted vs the volume fraction of the large cubes and vs the volume fraction of the small cubes for a mixture of side ratio 3. The different curves in the figures are computed at constant fugacity of the small cubes. In Fig. 3, we plot the fugacity of the large cubes versus the volume fraction of the large cubes for a mixture of cubes with size 4×4×4 and 2×2×2. For a side ratio of 3, we observed that upon increasing the fugacity of the solvent (i.e., of the small particles), the slope of the curves of constant solvent fugacity tends to zero at the inflection point. For still higher solvent fugacity, we find *two* different volume fractions of the large cubes for the *same* fugacity of the large particles (see Fig. 1). In Fig. 2, we observe the same flattening of the isofugacity curves. For still higher solvent fugacity, we again find *two* different volume fractions of the small cubes for the *same* fugacity for the large cubes. This is exactly what we expect for a demixing transition. The critical point can now be derived from a global fit of all isofugacity curves. When we take this into account, we can sketch the demixing region, as shown in Fig. 1. As the cubes are equally likely to be found on all lattice sites in both phases (i.e., there is no sublattice ordering), the present phase transition corresponds most closely to liquid–liquid coexistence in an off-lattice system. The simulations in the demixing region are very time consuming and therefore we have not attempted to locate the binodal curve more accurately. For a side ratio of 2, we find no evidence for a similar flattening of the isofugacity curves and we did not find two different volume fractions of the large cubes for the same fugacity of the large particles. Thus we find no evidence for a demixing transition in the less asymmetric system. However, if instead of cubes, we consider platelets, with a comparable volume (6×6×2, instead of 4×4×4), we again observe demixing (see Figs. 4 and 5). This is plausible as the clustering of the particles is controlled by depletion forces. When two large particles are brought into contact, the volume accessible to the small particles increases by an amount that is proportional to the diameter of the small particles and the area of contact of the large particles. The resulting gain in entropy of

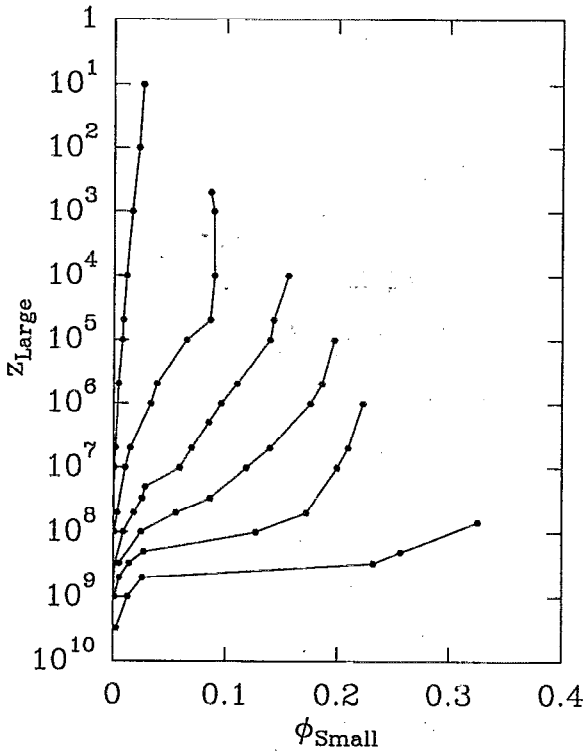

FIG. 2. The fugacity of the large cubes (size 6×6×6) vs the volume fraction of the small cubes at different fugacities (z_s=0, 100, 500, 1×10^3, 1.5×10^3, 2×10^3, and 5×10^3) of the small particles (size 2×2×2).

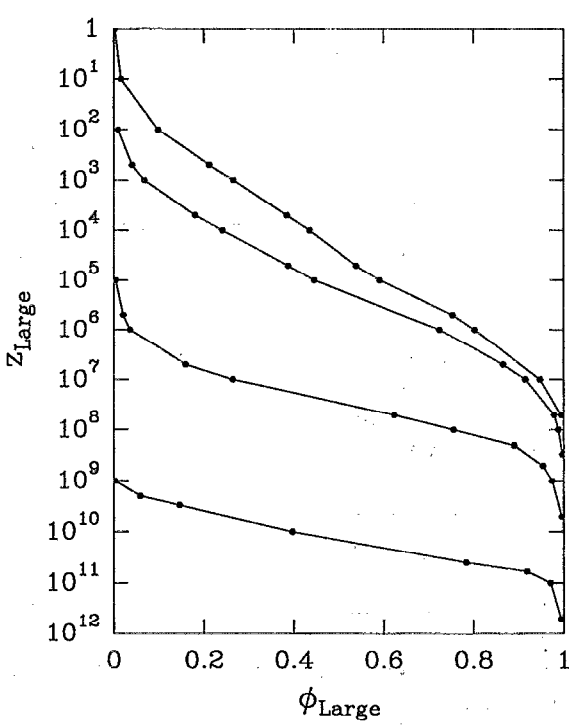

FIG. 3. The fugacity of the large cubes (size 4×4×4) vs the volume fraction of the large cubes at different fugacities (z_s=100, 1×10^3, 1×10^4, and 1×10^5) of the small particles (size 2×2×2).

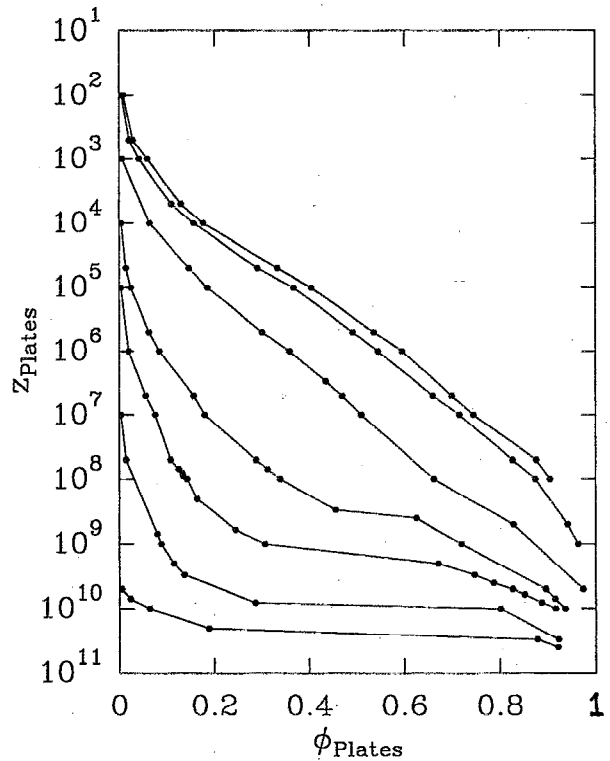

FIG. 4. The fugacity of the platelets (size 6×6×2) vs their volume fraction at different fugacities (z_s=5×10^2, 10^3, 10^4, 5×10^4, 10^5, 2×10^5, and 5×10^5) of the small particles (cubes of size 2×2×2).

the solvent is the driving force that makes the large particles cluster. The larger the surface-to-volume ratio of the large particles, the stronger is the tendency to demix.

In a two-dimensional mixture of squares with size 6×6 and 2×2, we did not find demixing. At the same "volume ratio," but with rods of size 18×2 instead of the large squares, the system appeared to approach a spinodal, but we were not able to reach it.

III. SIMULATIONS OF AN ATHERMAL POLYMER

The driving force that makes the particles cluster depends on the surface-to-volume ratio of the large particles. This argument should apply not only to rigid particles, such as rods and disks, but also to flexible particles, such as linear polymers. We therefore also looked for entropic demixing in an athermal polymer solution. In fact, in this case, we did not study the demixing directly. Rather, we looked for a closely related phenomenon, namely, the solvent-induced collapse of an isolated polymer. This collapse signals the transition from the good-solvent to the poor-solvent regime. There are compelling theoretical arguments to assume that a polymer collapse must occur in an athermal polymer solution when the polymer–solvent interaction is *nonadditive*.[11] In order to investigate if such a collapse can occur in an "additive" athermal polymer solution, we performed simulations of a single hard-core polymer in a solvent of cubes, where the size of the cubic monomers of the polymer is the same as the size of the solvent molecules, namely, 2×2×2 in units of the lattice

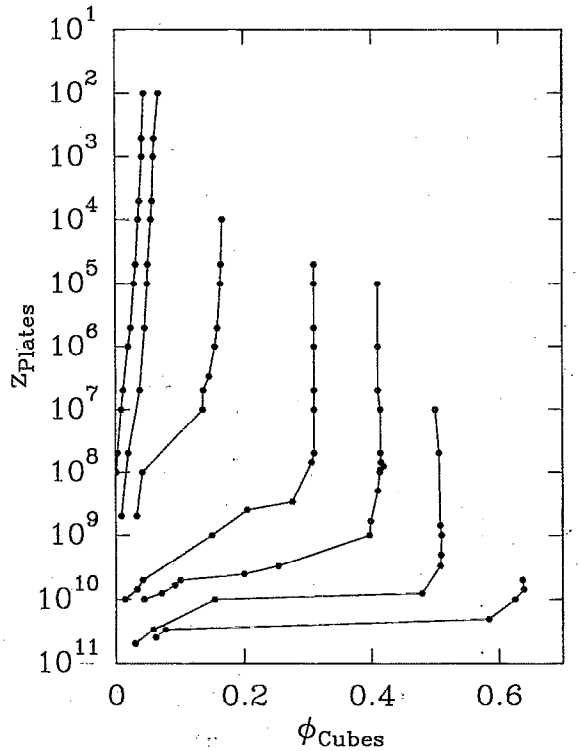

FIG. 5. The fugacity of the platelets (size 6×6×2) vs volume fraction of the small cubes at different fugacities ($z_c = 5\times10^2$, 10^3, 10^4, 5×10^4, 10^5, 2×10^5, and 5×10^5) of the small particles (cubes of size 2×2×2).

spacing. For the simulation of the hard-core polymer in a solvent, we used the configurational bias Monte Carlo (CBMC) method[15] for generating polymer conformations and the GCMC method for the solvent. Thus, we performed

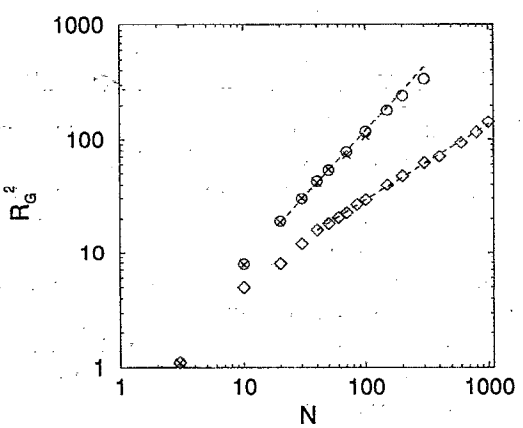

FIG. 6. The mean square of the radius of gyration (R_g^2) of a polymer with cubic monomers (size 2×2×2) with and without solvent (cubes of size: 2×2×2) vs the number of segments. Average solvent volume fraction 0.0 (circles), 0.3 (crosses), and 0.7 (open diamonds). Note that R_g^2 scales as $N^{2\nu}$ with the number of monomers (N). For the two low density runs, we find $\nu=0.56\pm0.02$ (for a polymer in a good solvent $\nu\sim0.58$). The high density run yields $\nu=0.34\pm0.02$. For a collapsed polymer, we expect "Euclidian" scaling $\nu=1/3$.

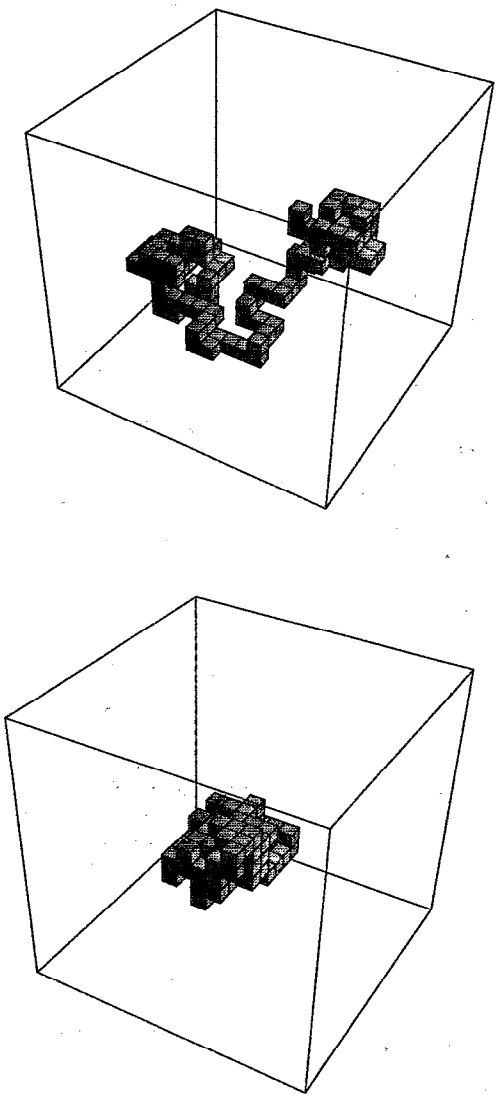

FIG. 7. A snapshot of conformation of a hard-core lattice polymer ($N=100$) *without* hard-core solvent (top) and in a solution of hard-core monomers with a volume fraction of 0.7 (bottom). Note the solvent-induced collapse.

the simulations on a system with fixed volume and temperature and at constant chemical potential of the solvent. The following trial moves have been performed:

(i) random displacement of a solvent molecule in the box;

(ii) removal or insertion of a solvent molecule;

(iii) regrowing a fraction of the polymer at either end of the chain;

(iv) regrowing a fraction of the polymer that does not include a free chain-end.

The last trial move was essential for a faster equilibration of the polymer and is explained in more detail in Appendices B and C. The dependence of the radius of gyration R_g on the number of monomers N is shown in Fig. 6 at different chemical potentials of the solvent. Figure 6 shows that when the chemical potential, and hence the volume frac-

tion of the solvent, is increased, the polymer undergoes a collapse transition. We find that the square of the radius of gyration R_g^2 scales as $N^{2\nu}$. For the two low chemical potentials that correspond to solvent volume fractions of 0 and about 0.3, we find $\nu=0.56\pm0.02$, which corresponds to the case of a polymer in a good solvent ($\nu\approx0.58$). For high chemical potential (average solvent volume fraction of 0.7), we find $\nu=0.34\pm0.02$. For a collapsed polymer we expect "Euclidian" scaling $\nu=1/3$. Figure 7 shows the very drastic change in the polymer shape when we go to high chemical potential of the solvent.

IV. VIRIAL EXPANSIONS FOR A BINARY MIXTURE OF HARD PARALLEL CUBES

A. Continuous system—behavior of $g_{22}(r)$ for $y\rightarrow0$

In order to gain a better understanding of the physical origin of phase separation in a hard-cube mixture, we analyzed the density expansions of the pair-distribution function of a closely related model, viz., parallel hard cubes off lattice. For the one-component parallel hard-cube model, the virial expansion of the pressure and the pair correlation function has been reported in the literature[16–18] up to terms of order ρ^7. Here we consider the virial expansion of the same quantities for the binary mixture. For two cubes with side length σ_1 and σ_2 at $\mathbf{r}_1$ and $\mathbf{r}_2$, the Mayer function is defined by

$$f_{12}(\mathbf{r}_1,\mathbf{r}_2)=-\prod_{i=1}^{3}\Theta(\sigma_{12}-|r_{1,i}-r_{2,i}|), \tag{1}$$

where $\Theta(x)$ is the Heavyside step function and $\sigma_{12}=(\sigma_1+\sigma_2)/2$. We computed the virial coefficients, up to the fourth, for the pair distribution function of the large particles, i.e., $g_{22}(x,y,z)$, as the latter quantity is expected to show evidence of incipient clustering that precedes demixing. If we define $\phi\equiv\phi(x,y,z)$ as the potential energy of a pair of particles, one at the origin and the other at (x,y,z), the virial expansion for $g_{22}(x,y,z)\exp(\beta\phi)$ in the densities ρ_1 and ρ_2 is[19]

The diagrams consist of circles and bonds. The circles represent the particle coordinates and the sizes of the circles denote the sizes of the particles. Open circles correspond to coordinates that are not integrated over; the black circles represent the variables of integration. The bonds between the circles are associated with the Mayer function. For example, the first diagram in the pair distribution function denotes

$$\int d\mathbf{r}_3\, f_{13}(\mathbf{r}_1,\mathbf{r}_3)f_{23}(\mathbf{r}_2,\mathbf{r}_3), \tag{3}$$

where particles 1 and 2 are large cubes and particle 3 is a small cube. Note that the three-dimensional integral factorizes into a product of three one-dimensional integrals. We calculated $g_{22}(\sigma_2,\sigma_2,\sigma_2)\exp(\beta\phi)$ and $g_{22}(0,0,\sigma_2)\exp(\beta\phi)$ up to the fourth virial coefficient. The expressions for these pair distribution functions in terms of the packing fractions $\eta_1=\sigma_1^3\rho_1$ and $\eta_2=\sigma_2^3\rho_2$ are

$$\begin{aligned} g_{22}(\sigma_2,\sigma_2,\sigma_2)\exp(\beta\phi) &= 1+\eta_1+\eta_2+\eta_1^2\left(-6+\frac{3}{\lambda}+\frac{3}{2\lambda^2}+\frac{1}{4\lambda^3}\right)\\ &\quad+\eta_1\eta_2\left(-\frac{3\lambda}{4}-1-\frac{3}{4\lambda}\right)+\eta_2^2\left(-\frac{5}{4}\right), \end{aligned} \tag{4}$$

$$\begin{aligned} g_{22}(0,0,\sigma_2)\exp(\beta\phi) &= 1+\eta_1\left(1+\frac{1}{\lambda}+\frac{1}{\lambda^2}\right)+4\eta_2+\eta_1^2\left(\frac{1}{\lambda}+\frac{5}{\lambda^2}+\frac{6}{\lambda^3}+\frac{1}{2\lambda^4}\right)\\ &\quad+\eta_1\eta_2\left(\frac{\lambda^2}{4}-2\lambda+5+\frac{11}{\lambda}+\frac{19}{4\lambda^2}\right)+9\eta_2^2, \end{aligned} \tag{5}$$

where λ is equal to σ_1/σ_2. For cubes facing each other $(0,0,\sigma_2)$, the divergence in $g_{22}(x,y,z)$ for $\lambda\rightarrow0$ already appears in the third virial coefficient, while for cubes diagonal to each other $(\sigma_2,\sigma_2,\sigma_2)$, the divergence only appears at the fourth virial coefficient. This is plausible because depletion forces are stronger when the area of contact of the large particles is larger. Thus, in the first case, the depletion effect is stronger. In Table I, the values of the one-dimensional integrals are listed that correspond to the graphs.

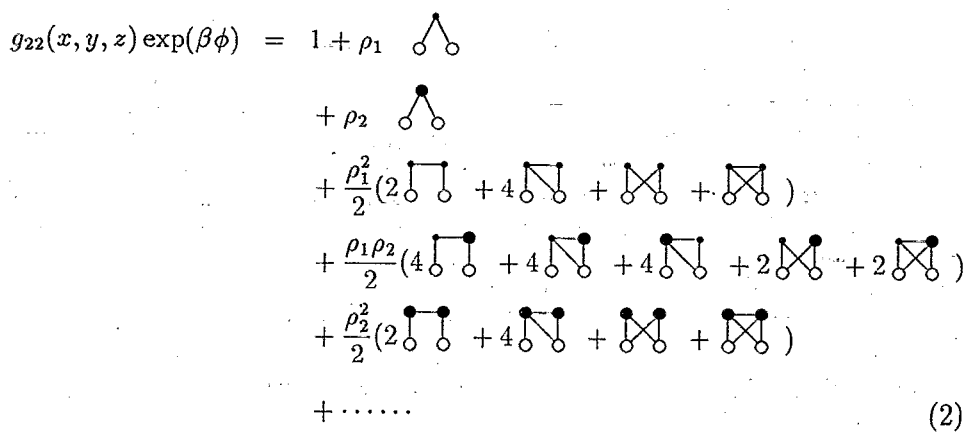

(2)

TABLE I. Values of the one-dimensional integrals that correspond to the graphs with $\sigma_{12}=\frac{1}{2}(\sigma_1+\sigma_2)$.

graph	value for $x=\sigma$	value for $x=0$
	σ_1	$2\sigma_{12}$
	σ_2	$2\sigma_2$
	$-2\sigma_1^2$	$-\sigma_1^2-2\sigma_1\sigma_2$
	$-\frac{1}{2}\sigma_1^2-\frac{1}{2}\sigma_2^2-\sigma_1\sigma_2$	$\frac{1}{2}\sigma_1^2-\frac{3}{2}\sigma_2^2-2\sigma_1\sigma_2$
	$-2\sigma_2^2$	$-3\sigma_2^2$
	$\sigma_1^2+\frac{1}{2}\sigma_1\sigma_2$	$\sigma_1^2+2\sigma_1\sigma_2$
	$\frac{1}{2}\sigma_1^2+\sigma_1\sigma_2$	$-\frac{1}{2}\sigma_1^2+\frac{3}{2}\sigma_2^2+2\sigma_1\sigma_2$
	$\frac{1}{2}\sigma_2^2+\sigma_1\sigma_2$	$-\frac{1}{2}\sigma_1^2+\frac{3}{2}\sigma_2^2+2\sigma_1\sigma_2$
	$\frac{3}{2}\sigma_2^2$	$3\sigma_2^2$
	σ_1^2	$4\sigma_{12}^2$
	$2\sigma_1\sigma_2$	$4\sigma_{12}\sigma_2$
	σ_2^2	$4\sigma_2^2$
	$-\sigma_1^2$	$-\sigma_1^2-2\sigma_1\sigma_2$
	$-2\sigma_1\sigma_2$	$\frac{1}{2}\sigma_1^2-\frac{3}{2}\sigma_2^2-2\sigma_1\sigma_2$
	$-\sigma_2^2$	$-3\sigma_2^2$

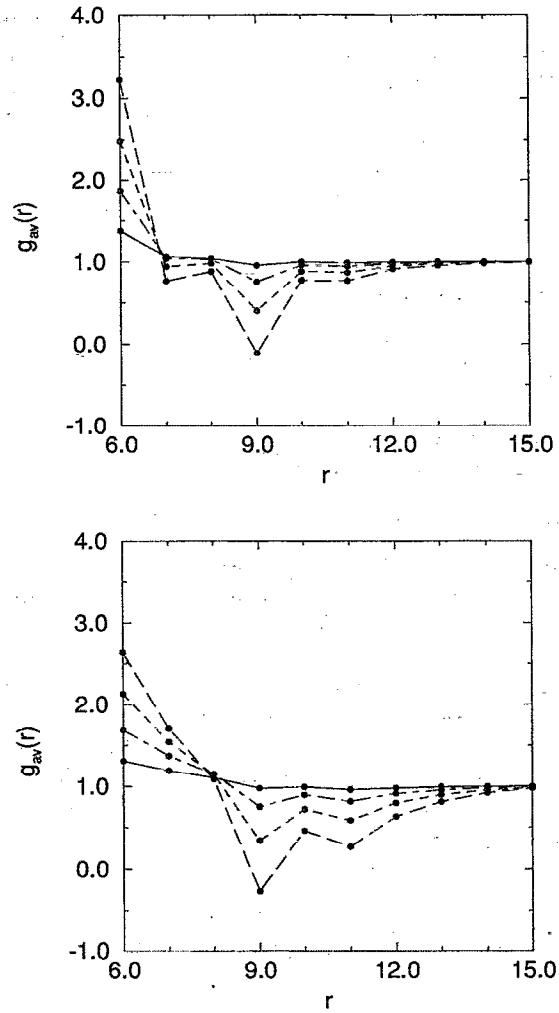

FIG. 8. (Top) $g_{av}(r)$ vs r for a binary mixture of cubes (size 6×6×6 and 2×2×2) at equal packing fractions for the large and small cubes. (Bottom) $g_{av}(r)$ vs r for a system with only large cubes. In both pictures, the total packing fraction η is (solid line) $\eta=0.2$; (dashed–dotted) $\eta=0.4$; (dashed) $\eta=0.6$; and (long dashed) $\eta=0.8$.

B. Discrete systems—computation of $g_{22}(\mathbf{r})$

In order to make contact with the simulations described before, we also calculated the virial coefficients of $g_{22}(\mathbf{r})$ for the discrete model of a binary hard-cube mixture, i.e., a cubic lattice with parallel hard cubes occupying σ_1^3 or σ_2^3 lattice points. As the virial coefficients are computed by counting lattice sites, it was necessary to fix the absolute size of the cubes rather than just their size ratio. We computed $g_{22}(\mathbf{r})$ for a system of cubes with size ratio 3 and size ratio 2. In both cases, the diameter of the small cubes was equal to 2. In Tables II and III, the values for the one-dimensional integrals are listed that correspond to the graphs. We define a suitably averaged pair-distribution function by averaging over all values of $g_{22}(r)$ on the surface of a cube with side length r, analogous to the one used in Ref. 18.

$$g_{av}(r)=\frac{1}{(2r+1)^2}\sum_{x=-r}^{r}\sum_{y=-r}^{r} g_{22}(x,y,z=r). \tag{6}$$

In Figs. 8 and 9, we have plotted $g_{av}(r)$ vs r at different packing fractions and different size ratios. We see in Fig. 8 that for the binary mixture of hard parallel cubes with sizes $\sigma_1=2$ and $\sigma_2=6$, $g_{av}(r=\sigma_2)$ for the large cubes is significantly higher than for a system with only large cubes at the same total packing fraction. Thus the addition of small cubes has the effect that the large cubes tend to stick together. On the contrary, for a binary mixture of cubes with size length $\sigma_1=2$ and $\sigma_2=4$, $g_{av}(r=\sigma_2)$ is somewhat lower than for the pure system and the large particles are not prone to clustering when small cubes are added (see Fig. 9). However, if we consider a mixture of parallel platelets (size 6×6×2) and cubes (size 2×2×2) with a volume ratio comparable to the previous system, we see in Table V that $g_{av}(r=\sigma_2)$ in the binary mixture is larger than for a pure system with only platelets. This can be explained by the larger surface-to-volume ratio of the platelets. The depletion effect is stronger when the area of contact of the two large particles that stick

TABLE II. The values of the one-dimensional integrals that correspond to the graphs for $g_{22}(r)\exp(\beta\phi)$ are given for a discrete binary mixture of hard cubes with side lengths 6 and 2 in. units of the lattice spacing.

r															
0	7	11	-19	-47	-91	19	47	47	91	49	77	121	-19	-47	-91
1	6	10	-18	-46	-90	17	45	41	85	36	60	100	-16	-40	-80
2	5	9	-15	-43	-87	14	42	34	78	25	45	81	-13	-33	-69
3	4	8	-12	-39	-82	11	38	27	70	16	32	64	-10	-26	-58
4	3	7	-9	-34	-75	8	33	20	61	9	21	49	-7	-19	-47
5	2	6	-6	-28	-66	5	27	13	51	4	12	36	-4	-12	-36
6	1	5	-3	-21	-55	2	20	6	40	1	5	25	-1	-5	-25
7		4	-1	-15	-45		14		30			16			-16
8		3		-10	-36		9		21			9			-9
9		2		-6	-28		5		13			4			-4
10		1		-3	-21		2		6			1			-1
11				-1	-15										
12					-10										
13					-6										
14					-3										
15					-1										

together is larger. The averaged $g_{av}(r)$ is now obtained by averaging over all values for $g_{22}(r)$ on the surface of a platelet. In Table II and IV, the values for the one-dimensional integrals are listed that correspond to the graphs that are needed to compute $g(r)$ in this binary system of platelets and cubes. In Table VI, we see that for a two-dimensional system of squares with a side ratio of 3, $g_{av}(r=\sigma_2)$ is not larger for a binary mixture, compared with a pure system at the same total packing fraction.

V. CONCLUSIONS

In Sec. IV A, we showed that for a binary hard-core mixture of parallel hard cubes with side lengths σ_1 and σ_2, the pair distribution function for the large particles diverges at contact in the limit $\sigma_1/\sigma_2 \to 0$. Thus, we expect, on the basis of these calculations, a demixing transition for mixtures with sufficiently large size asymmetry. In a binary mixture of hard spheres with diameters σ_1 and σ_2, a similar divergence of the pair distribution function was found within the Percus–Yevick approximation in the limit $\sigma_1/\sigma_2 \to 0$.[20] By computer simulations, we do indeed see a demixing transition in a lattice model of such a mixture provided that the size asymmetry of the large and small particles is larger than 2. When the size ratio of the cubes equals 3, we found clear evidence of a demixing transition in our simulations, but such demixing was not observed for a cube side ratio of 2. However, if we consider platelets instead of the large cubes of comparable volume, the system will again become unstable with respect to phase separation. This can be explained by a stronger depletion effect for platelets. In a two-dimensional mixture of squares of size 6×6 and 2×2, we found no evidence for demixing. At the same "volume ratio," but with rods of size 18×2 instead of the large squares, the system appeared to approach a spinodal. The simulations support the theoretical predictions by Sanchez[21] of the existence of entropy-driven demixing in binary solutions. He

TABLE III. The values of the one-dimensional integrals that correspond to the graphs for $g_{22}(r)\exp(\beta\phi)$ are given for a discrete binary mixture of hard cubes with side lengths 4 and 2 in. units of the lattice spacing.

r															
0	5	7	-13	-23	-37	13	23	23	37	25	35	49	-19	-23	-37
1	4	6	-12	-22	-36	11	21	19	33	16	24	36	-10	-18	-30
2	3	5	-9	-19	-33	8	18	14	28	9	15	25	-7	-13	-23
3	2	4	-6	-15	-28	5	14	9	22	4	8	16	-4	-8	-16
4	1	3	-3	-10	-21	2	9	4	15	1	3	9	-1	-3	-9
5		2	-1	-6	-15		5		9			4			-4
6		1		-3	-10		2		4			1			-1
7				-1	-6										
8					-3										
9					-1										

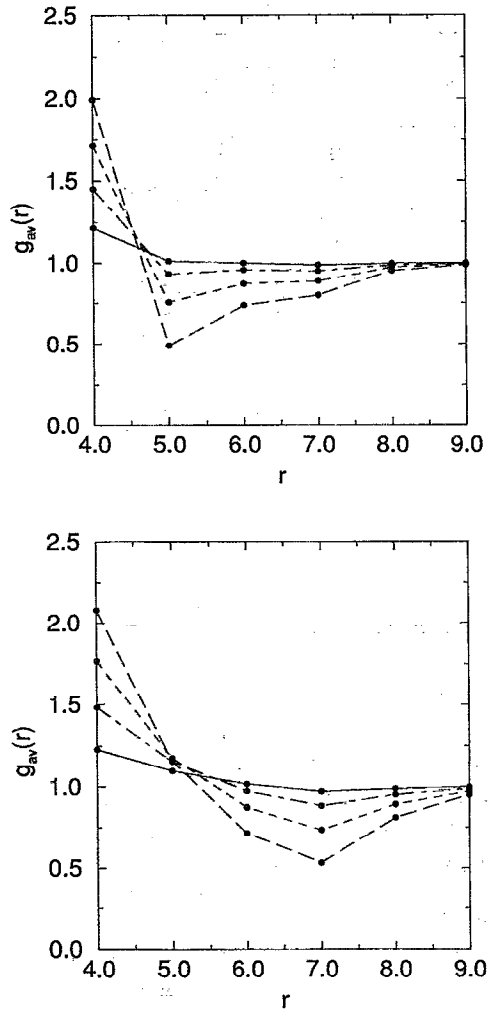

FIG. 9. (Top) $g_{av}(r)$ vs r for a binary mixture of cubes (size 4×4×4 and 2×2×2) at equal packing fractions for the large and small cubes. (Bottom) $g_{av}(r)$ vs r for a system with only large cubes. In both pictures, the total packing fraction is (solid line) η=0.2; (dashed–dotted) η=0.4; (dashed) η=0.6; and (long dashed) η=0.8.

showed that the compressible nature of binary solutions and differences in the pure-component equation of state properties play an important role in solution thermodynamics. For instance, the description of phase stability separates into a constant volume (incompressible) contribution and a volume fluctuation (compressible) contribution. In most theories, the latter quantity has been neglected. However, this is only correct when the pure components have identical equation of state properties and interact neutrally with one another. When we take volume fluctuations into account, the system is able to explore other regions of configuration space corresponding to larger volumes and lower free energies. A compressible solution is, hence, thermodynamically less stable than an incompressible solution. In binary hard-core mixtures with sufficiently large size asymmetry, the equation of state properties of the pure components will be sufficiently different, so that compressibility contributions will play an important role in the description of phase stability.

In this context, it is interesting to consider what happens in the high-density limit. In that case, every lattice site will be occupied by either a large or a small particle. This can only be achieved if all particles order on a sublattice. However, once this spatial ordering has taken place, there is no longer any gain in entropy associated with demixing. Hence, at high densities, the system will mix again. In Sec. IV B, we computed the averaged pair distribution function at contact $g_{av}(\sigma_2)$ for the large particles up to the fourth virial coefficient for several systems. We found that a comparison of the computed values for $g_{av}(\sigma_2)$ for a binary mixture and for a pure system with only large particles at the same total packing fraction provides an indication of the tendency of the system to demix. In particular, we found a larger value of $g_{av}(\sigma_2)$ only for the binary mixture of cubes with size ratio 3 and the mixture of platelets and small cubes. By computer simulations, we indeed observed *only* in these systems a de-

TABLE IV. The values of the one-dimensional integrals that correspond to the graphs for $g(r)\exp(\beta\phi)$ are shown here for a discrete system of hard cubes with side length 2 in. units of the lattice spacing.

r	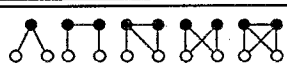				
0	3	-7	7	9	-7
1	2	-6	5	4	-4
2	1	-3	2	1	-1
3	0	-1	0	0	0

TABLE V. The values for the averaged $g_{av}(r=6)$ are tabulated for a discrete system of hard parallel platelets of size 6×6×2 and packing fraction η_2 and with cubes of side length 2 and packing fraction η_1.

$\eta_2+\eta_1$	η_1=0.0	η_1=0.2	η_1=0.4	η_1=0.6	η_1=0.8
0.1	1.088 83				
0.2	1.180 29				
0.3	1.274 36	1.465 28			
0.4	1.371 05	1.559 50			
0.5	1.470 37	1.656 35	1.981 81		
0.6	1.572 30	1.755 81	2.078 80		
0.7	1.676 85	1.857 89	2.178 42	2.638 43	
0.8	1.784 02	1.962 60	2.280 65	2.738 19	
0.9	1.893 81	2.069 92	2.385 51	2.840 58	3.435 13

TABLE VI. The values for the averaged $g_{av}(r=6)$ are tabulated, for a two-dimensional discrete system of hard squares of size 6×6 and packing fraction η_2 and squares with side length 2 and packing fraction η_1.

$\eta_2+\eta_1$	η_1=0.0	η_1=0.2	η_1=0.4	η_1=0.6	η_1=0.8
0.1	1.116 93				
0.2	1.251 90				
0.3	1.404 91	1.366 01			
0.4	1.575 97	1.533 91			
0.5	1.765 08	1.719 85	1.670 47		
0.6	1.972 22	1.923 84	1.871 30		
0.7	2.197 41	2.145 86	2.090 17	2.030 32	
0.8	2.440 65	2.385 94	2.327 08	2.264 08	
0.9	2.701 92	2.644 05	2.582 04	2.515 87	2.445 56

mixing transition. For the mixture of cubes with size ratio 2 and the two-dimensional system of hard squares, we found a lower value for the pair distribution functions at contact, compared to the pure systems. In the simulations of these systems, we found no phase separation. Thus the calculation of the pair distribution functions of the large particles at contact gives a rough estimate whether the mixture is stable against phase separation.

Finally, we performed simulations of a hard-core polymer in a hard-core solvent. By increasing the solvent fugacity in this athermal polymer solution, we can make the polymer collapse. It is important to note that the collapse of the polymer chain in a solvent is, in a sense, counterintuitive. If one considers exclusively the polymer chain, there is a large amount of entropy lost by the collapsed polymer. However, the increase in entropy of the solvent molecules overrides this apparent loss. The observation of such a solvent-induced polymer collapse immediately implies the existence of a demixing transition in this athermal polymer solution. Also in this case, the polymer will expand again at high densities, as the gain in entropy associated with the polymer collapse will disappear for the same reason as mentioned above. The present simulations support existing theoretical predictions of the occurrence of entropy-driven demixing in polymer blends and solutions. In particular, Freed and Bawendi[22] have argued on theoretical grounds that polymer blends in which monomers extend over several lattice sites, and therefore have different sizes and shapes, can demix. Similarly, Sanchez[21] has considered the inclusion of compressibility effects into the theory of polymer mixtures. Again, an entropy-driven phase separation is predicted. Hariharan and Kumar[23] studied the effect of compressibility in an athermal mixture of short and long chains in the vicinity of a hard wall by computer simulations. In such a mixture, the short chains (which lose less entropy per segment) partition preferentially to the surface in order to minimize the entropy loss due to the presence of the wall, and Hariharan and Kumar find that the compressibility of the mixture enhances this effect. Simulations of athermal polymer solutions have been reported before,[24] but a purely entropic polymer collapse has, to our knowledge, not been observed.

ACKNOWLEDGMENTS

The work of the FOM Institute is part of the scientific programme of FOM and is supported by the Nederlandse Organisatie voor Wetenschappelijk Onderzoek (NWO).

APPENDIX A

In a dense system of small cubes, random displacement of a large particle is difficult. To overcome this problem, we remove the small particles that hinder the displacement of the large particle and reinsert them into the space vacated by the large particles. The algorithm for moving a big particle goes as follows:

(1) choose a random displacement of a large particle;
(2) if the large particle at its new position overlaps with another large particle, this move is immediately rejected;
(3) if there is no such overlap, the n small particles that overlap with the large particle at its new position are determined;
(4) the n small particles are inserted into the volume vacated by the displacement of the large particle to its new position.

The insertion of the n small particles into the free volume is not simple as the probability of random insertion of n particles into a restricted volume is small. We therefore used a method similar to the one proposed by Siepmann and Frenkel for polymer systems.[25] When $i-1$ small particles have already been inserted, we attempt to insert the ith particle.

(i) For all k lattice sites that become free after displacement of a large particle, the external Boltzmann factor $\exp(-\beta u_{w_i})$ for inserting a small particle on that lattice point is computed. The external energy is the energy of the small particle due to interaction with all the large and small particles in the system. For hard-core particles, this Boltzmann factor is either zero in the case of overlap, or one when there is no overlap with other particles.

(ii) One of the k lattice sites, say $\mathbf{w}_i$, is selected with a probability

$$P_{\mathbf{w}_i}=\frac{\exp(-\beta u_{\mathbf{w}_i})}{Z_{\{\mathbf{w}\}_i}} \tag{A1}$$

with

$$Z_{\{\mathbf{w}\}_i}=\sum_{j=1}^{k} \exp(-\beta u_{\mathbf{w}_j}). \tag{A2}$$

The subscript $\{\mathbf{w}\}_i$ means that $\mathbf{w}_i$ is one of the k trial lattice sites, i.e. $\mathbf{w}_i \in \{\mathbf{w}\}_i$. The ith small particle is inserted at this lattice point and the corresponding partial "Rosenbluth weight" is stored

$$\omega_i=\frac{Z_{\{\mathbf{w}\}_i}}{k}. \tag{A3}$$

(iii) These steps are repeated until all n small particles have been inserted.

Within the configurational bias method, we used the detailed balance condition in the Metropolis form[15] to determine the probability of acceptance

$$acc(a|b)=\min\left[1, \frac{P_a/\exp(-\beta U_a)}{P_b/\exp(-\beta U_b)}\right], \tag{A4}$$

where P_a and P_b are, respectively, the probabilities that the system is in the original conformation a and in the new conformation b, and U_a and U_b are the total energies of these two conformations. The probability that the system is found in the new conformation b is equal to the probability of inserting the n small particles into the free volume

$$P_b=\prod_{i=1}^{n} \frac{\exp(-\beta u_{\mathbf{w}_{i_b}})}{Z_{\{\mathbf{w}\}_{i_b}}} \tag{A5}$$

Since $U_b = \Sigma_{j=1}^{k} u_{\mathbf{w}_{j_b}} + u_{\mathbf{w}_{\text{large},b}} + u_{\mathbf{w}_{\text{rest}}}$ and the Rosenbluth factor is equal to

$$\mathscr{W}_b = \prod_{i=1}^{n} \frac{Z_{\{\mathbf{w}\}_{i_b}}}{k}, \tag{A6}$$

we arrive at

$$P_b/\exp(-\beta U_b) = \{\exp[-\beta(u_{\mathbf{w}_{\text{large},b}} + u_{\mathbf{w}_{\text{rest}}})]k^n \mathscr{W}_b\}^{-1}. \tag{A7}$$

Substitution of Eq. (A7) in Eq. (A4) gives

$$acc(a|b) = \min\left\{1, \frac{\mathscr{W}_b}{\mathscr{W}_a} \exp[-\beta(u_{\mathbf{w}_{\text{large},b}} - u_{\mathbf{w}_{\text{large},a}})]\right\}. \tag{A8}$$

APPENDIX B

For a faster equilibration of the polymer during simulations, we regrow parts in the middle of the chain with a modified CBMC method.[14] In this case, we have to take care that the end parts of the chain will be connected again. We shall first describe how we regrow a part in the middle of the chain within a modified Rosenbluth scheme. Then we shall describe how to implement this in a CBMC scheme, such that detailed balance is satisfied. The regrowth algorithm goes as follows:

(1) Choose a part at random in the middle of the chain, say L segments, and remove this part.
(2) Regrow this part of the chain segment by segment. When we have already grown $i-1$ segments, we try to add segment i. For all k possible directions of segment i, we compute the external and the internal energies. Note that the number of trial directions k is equal to 6 on a cubic lattice. The external energy is the energy of the trial segment due to interaction with the polymer and the solvent molecules. Since we have only hard-core interactions in our system, the external energy is either zero for an unoccupied lattice site or infinity for an occupied one. The internal energy is equal to the number of ideal random walks $N_{\mathbf{w}_i}^{\text{RW}}$ that connect the trial segment with the other end part of the chain in $L-i$ steps. This number can be calculated easily (see Appendix C), and for the sake of efficiency, we have tabulated these numbers. The role of this internal energy is to ensure that the end parts of the chain will be connected again.
(3) Select one of the trial segments, say $\mathbf{w}_i$, with a probability

$$P_{\mathbf{w}_i} = \frac{N_{\mathbf{w}_i}^{\text{RW}} \exp(-\beta u_{\mathbf{w}_i})}{Z_{\{\mathbf{w}\}_i}}, \tag{B1}$$

where we have defined

$$Z_{\{\mathbf{w}\}_i} = \sum_{j=1}^{k} N_{\mathbf{w}_j}^{\text{RW}} \exp(-\beta u_{\mathbf{w}_j}). \tag{B2}$$

The subscript $\{\mathbf{w}\}_i$ means that $\mathbf{w}_i$ is one of the segments of the trial directions, i.e., $\mathbf{w}_i \in \{\mathbf{w}\}_i$. We add this segment to the chain and store the corresponding partial "Rosenbluth weight"

$$\omega_i = \frac{Z_{\{\mathbf{w}\}_i}}{k}. \tag{B3}$$

We repeat steps (2) and (3) until the chain is connected again.

For the configurational bias method, we used the detailed balance condition in the Metropolis form given by Eq. (A4), where P_a and P_b are now, respectively, the probabilities that the part of the chain is in conformation a or b. The probability that the regrown part of the chain, consisting of L segments, has conformation b is equal to

$$P_b = \prod_{i=1}^{L} \frac{N_{\mathbf{w}_{i_b}}^{\text{RW}} \exp(-\beta u_{\mathbf{w}_{i_b}})}{Z_{\{\mathbf{w}\}_{i_b}}}. \tag{B4}$$

Since $U_b = \Sigma_{i=1}^{L} u_{i_b}$ and the Rosenbluth factor is equal to

$$\mathscr{W}_b = \prod_{i=1}^{L} \frac{Z_{\{\mathbf{w}\}_{i_b}}}{k}, \tag{B5}$$

we arrive at

$$P_b/\exp(-\beta U_b) = \frac{G_b}{k^L \mathscr{W}_b} \tag{B6}$$

with

$$G_b = \prod_{i=1}^{L} N_{i_b}^{\text{RW}}. \tag{B7}$$

Substitution of Eq. (B6) in Eq. ?? gives

$$acc(a|b) = \min(1, \mathscr{W}_b G_b^{-1}/\mathscr{W}_a G_a^{-1}). \tag{B8}$$

In other words, this modified configurational bias Monte Carlo (CBMC) scheme works as follows:

(1) generate a trial conformation for the selected part of the chain by using the Rosenbluth scheme, as described above;
(2) compute the Rosenbluth weights times the weight functions

$$\mathscr{W}_{\text{old}} G_{\text{old}}^{-1} \quad \text{and} \quad \mathscr{W}_{\text{trial}} G_{\text{trial}}^{-1}$$

(3) of the trial conformation and of the old conformation; accept the trial move with probability

$$\min(1, \mathscr{W}_{\text{trial}} G_{\text{trial}}^{-1}/\mathscr{W}_{\text{old}} G_{\text{old}}^{-1}).$$

APPENDIX C

The number of ideal random walks from lattice point (0,0,0) to lattice point $(\Delta x, \Delta y, \Delta z)$ in N steps can be computed as follows: we start with the expression for the number of possible ideal random walks consisting of N steps with a fixed number of steps in all directions

$$N^{\mathrm{RW}}(x,\bar{x},y,\bar{y},z,\bar{z};N)=\frac{N!}{x!\bar{x}!y!\bar{y}!z!\bar{z}!}. \tag{C1}$$

The number of steps in the positive x, y, and z directions are given by x, y, and z, while $\bar{x}$, $\bar{y}$, and $\bar{z}$ are the number of steps in the negative directions. Note that the sum of all steps must be equal to N,

$$x+\bar{x}+y+\bar{y}+z+\bar{z}=N. \tag{C2}$$

To obtain the required number of ideal random walks from (0,0,0) to $(\Delta x,\Delta y,\Delta z)$, we have to sum over the number of random walks with N steps with all possible values of x, $\bar{x}$, y, $\bar{y}$, z, and $\bar{z}$ subject to the constraints that

$$\Delta x=x-\bar{x},\quad \Delta y=y-\bar{y},\quad \Delta z=z-\bar{z}. \tag{C3}$$

The number of ideal random walks of N steps resulting in displacements Δx, Δy, and Δz in the x, y, and z directions then reduces to

$$N^{\mathrm{RW}}(\Delta x,\Delta y,\Delta z;N)=\sum_{\bar{x}=0}^{N^{-}-\bar{y}}\sum_{\bar{y}=0}^{N^{-}}\frac{N!}{\bar{x}!(\bar{x}+\Delta x)!\bar{y}!(\bar{y}+\Delta y)!(N^{-}-\bar{x}-\bar{y})!(N^{+}-\bar{x}-\bar{y})!} \tag{C4}$$

with $N^{-}=(N-\Delta x-\Delta y-\Delta z)/2$ and $N^{+}=(N-\Delta x-\Delta y+\Delta z)/2$.

[1] G. I. Kerley, J. Chem. Phys. **91**, 1204 (1989).
[2] A. de Kuijper, B. Smit, J. A. Schouten, and J. P. J. Michels, Europhys. Lett. **13**, 679 (1990).
[3] J. L. Lebowitz and J. S. Rowlinson, J. Chem. Phys. **41**, 133 (1964).
[4] E. B. Smith and K. R. Lea, Trans. Faraday Soc. **59**, 1535 (1963).
[5] B. J. Alder, J. Chem. Phys. **40**, 2724 (1964).
[6] A. Rotenberg, J. Chem. Phys. **43**, 4377 (1965).
[7] P. H. Fries and J. P. Hansen, Mol. Phys. **48**, 891 (1983).
[8] G. Jackson, J. S. Rowlinson, and F. van Swol, J. Phys. Chem. **91**, 4907 (1987).
[9] T. W. Melnyk and B. L. Sawford, Mol. Phys. **29**, 891 (1975).
[10] D. J. Adams and I. R. McDonald, J. Chem. Phys. **63**, 1900 (1975).
[11] D. Frenkel and A. A. Louis, Phys. Rev. Lett. **68**, 3363 (1992).
[12] T. Biben and J. P. Hansen, Phys. Rev. Lett. **66**, 2215 (1991).
[13] H. N. W. Lekkerkerker and A. Stroobants, Phys. Status Solidi A **195**, 387 (1993).
[14] T. Biben, Ph.D. thesis, Université Claude Bernard-Lyon 1, France, 1993.
[15] D. Frenkel, G. C. A. M. Mooij, and B. Smit, J. Phys. Condensed Matter **3**, 3053 (1991).
[16] T. R. Kirkpatrick, J. Chem. Phys. **85**, 3515 (1986).
[17] W. G. Hoover and A. G. De Rocco, J. Chem. Phys. **36**, 3141 (1962).
[18] W. G. Hoover and J. C. Poirier, J. Chem. Phys. **38**, 327 (1963).
[19] J. P. Hansen and I. R. McDonald, *Theory of Simple Liquids*, 2nd ed. (Academic, London, 1986).
[20] T. Biben and J. P. Hansen, Europhys. Lett. **12**, 347 (1990).
[21] I. C. Sanchez, Macromolecules **24**, 908 (1991).
[22] K. F. Freed and M. G. Bawendi, J. Phys. Chem. **93**, 2194 (1989).
[23] A. Hariharan and S. K. Kumar, J. Chem. Phys. **99**, 4041 (1993).
[24] A. Yethiraj and R. Dickman, J. Chem. Phys. **97**, 4468 (1992).
[25] J. I. Siepmann and D. Frenkel, Mol. Phys. **75**, 59 (1992).